



Non stoichiometric $\text{La}_{1-y}\text{FeO}_3$ perovskite-based catalysts as alternative to commercial three-way-catalysts? – Impact of Cu and Rh doping

Anke Schön, Jean-Philippe Dacquin, Pascal Granger*, Christophe Dujardin*

Université de Lille, ENSCL, Unité de Catalyse et Chimie du Solide, UMR CNRS 8181, Cité Scientifique Bât. C3, 59655 Villeneuve d'Ascq Cedex, France



ARTICLE INFO

Article history:

Received 29 November 2016

Received in revised form 14 April 2017

Accepted 8 June 2017

Available online 9 June 2017

Keywords:

Three-way catalyst

Rhodium

Perovskite

NO_x

Non-stoichiometric $\text{La}_{1-y}\text{Fe}_{1-x}\text{Cu}_x\text{O}_3$

ABSTRACT

A series of $\text{La}_{1-y}\text{Fe}_{1-x}\text{Cu}_x\text{O}_3$ catalysts with $y = 0, 0.33$ and $x = 0, 0.17, 0.2$ was prepared by a conventional sol-gel method. The catalytic activity in Three-Way Catalysis (TWC) of perovskite-based solids was compared to a commercial reference which contains Pd and Rh. The combination of Lanthanum-deficient synthesis and iron substitution by copper in LaFeO_3 solid largely contributed to the enhancement of oxidation reactions especially for CO and propene whereas Rh doping activated the NO reduction in stoichiometric conditions. A better yield to nitrogen was obtained with much lower formation of ammonia at high temperature compared to the commercial reference. The characterization of perovskite-based catalyst (XRD, XPS, BET, H_2 -TPR) highlighted the specific properties due to Lanthanum-deficient synthesis and iron substitution by copper in LaFeO_3 .

© 2017 Elsevier B.V. All rights reserved.

1. Introduction

An interesting challenge was highlighted in a recent report regarding the need to develop alternatives to the use of critical raw materials such as precious metals [1]. The potential of perovskite-based materials was largely illustrated in the literature for environmental applications [2]. The viewpoint given by the authors was reasonably supported by considerable developments in the solid preparation with enhancement of their textural properties which widens the panel of applications especially in post-combustion catalysis. Numerous investigations pointed out the advantage of three-dimensional perovskite type structure using templating methods for their preparation with subsequent improvement in specific surface area and pore structure [3,4]. However the peculiarities of perovskites ABO_3 are not only restricted to their textural properties. Their typical structure can accommodate a wide variety of atoms in B or A sites, tuning their redox properties and stability through coordination number and vacancy control. Significant synergy effects on the catalytic activity can be obtained according to this methodology [5]. Obviously, significant outcomes were recently obtained showing that strontium-doped perovskites can be efficient platinum substitutes for Diesel Oxidation Catalysts (DOC) [6]. These catalysts can be found upstream in Lean- NO_x trap

(LNT) systems and could be very cost-efficiency. In large excess of oxygen, the redox properties of perovskites cannot be properly well-adjusted to oxidize both CO and unburnt hydrocarbon as well as reduce simultaneously and selectively NO_x into nitrogen. This can limit the use of such perovskite-based catalysts for lean burn after-treatment systems. Constantinou et al. illustrated the use of perovskite structures for NO_x storage reduction systems running in transient lean/rich regime but they concluded that lower performances were obtained compared to conventional LNT formulations [7]. As a matter of fact, outstanding progresses were achieved in three-way catalysis (TWC) with end-of-pipe technologies typically running near stoichiometric conditions [8–10]. The concept of self-regenerating catalysts developed by Nishihata et al. [11] gave rise to significant practical outcomes. These authors found that reversible surface processes taking place on Pd-perovskite during lean/rich cycles near stoichiometric conditions can considerably enhance the resistance to particle sintering compared to conventional TWC using alumina as support. The mobility of Pd species is put into evidence especially at high temperature. Isolated Pd species go out and return into their initial position inside the perovskite lattice between reductive and oxidative atmosphere typically encountered in TWC catalysis. This behavior can suppress the growth of precious metal particles occurring generally during high temperature ageing [10,12]. The authors also investigate this concept of “intelligent catalyst” in the case of platinum and rhodium. They finally propose different criteria for designing universally the self-regenerative function in the case of noble metals-doped perovskite [13]. Such development is claimed by Daihatsu Motor with typi-

* Corresponding authors.

E-mail addresses: pascal.granger@univ-lille1.fr (P. Granger), christophe.dujardin@ensc-lille.fr (C. Dujardin).

cal $A_xB_{(1-y)}Pd_yO_{3+\delta}$ solids ($x > 1$) [14]. Another recent development involving perovskite for TWC is proposed by Clean Diesel Technologies with the embodiment of Pd(+1) in the perovskite in order to mimic rhodium's electronic configuration and catalytic properties in TWC [15]. However, all the findings are not univocal because a significant part of precious metal could remain embedded and is not accessible to the reactive atmosphere [16]. For instance, Zhou et al. obtained better performance for perovskite supported palladium instead of Pd-substituted perovskite as three-way catalysts because palladium can be more easily reduced in the former case. However their catalytic activity converges upon ageing which led the authors to conclude that Pd species deposited through an impregnation process can also migrate inside the perovskite lattice hence leading to a mixture of metallic palladium particles and isolated Pd cations [17]. It was also found that impregnated samples were also more selective to the production of nitrogen than doped-perovskites by precious metals [18]. Different features were reported on impregnated-Pt/LaFeO₃ and the authors attributed significant gain in NO reduction to an epitaxial growth of Pt particles on LaFeO₃ instead of the formation of subsurface oxidic Pt species due to their diffusion [19,20]. On the other hand the Cu-substituted ortho-ferrites were previously investigated for TWC applications and the highest catalytic activity for CO oxidation was observed for LaFe_{0.8}Cu_{0.2}O₃ catalyst [21]. Another approach for perovskite-based catalyst (typically ABO₃) consists of the tuning of surface concentration between A and B elements thanks to lanthanum-deficient synthesis [9]. Significant improvement of catalytic activity was demonstrated in the catalytic decomposition of N₂O [22] and applied more recently to CO oxidation on La_{0.8}FeO₃ solid [9].

This paper provides new perspectives with the development of lanthanum-deficient perovskites. The combination of copper insertion and optimization of lanthanum surface concentration is proposed in this study for Three-Way-Catalysis applications. Particular attention is paid to minimize the use of precious metal. Further incorporation of low amount of Rh can provide equivalent and even better performance than commercial three-way catalysts during the cold start engine especially for the conversion of NO_x.

2. Experimental

2.1. Catalyst preparation

A series of La_{1-y}Fe_{1-x}Cu_xO₃ (with $y=0$, 0.33 and $x=0.17$ and 0.2) were prepared according to a conventional citrate method as reported elsewhere [23,24]. The following precursor salts were used: La(NO₃)₃·6H₂O, Fe(NO₃)₃·6H₂O and Cu(NO₃)₂·2.5H₂O and citric acid supplied by Sigma Aldrich. The molar ratio of (La + Fe + Cu):Citric Acid = 1:1 was kept constant. After drying, the precursor was heated in a muffle furnace up to 200 °C for the exothermic decomposition of nitrates, then calcined in air for 8 h at 600 °C in a fixed bed reactor. Rh-doped perovskite sample was prepared by wet impregnation of calcined La_{0.67}Fe_{0.83}Cu_{0.17}O₃ from a solution of Rh(NO₃)₃ in order to get 0.1 wt.% Rh. The impregnated sample thus obtained was dried at 80 °C and then calcined in air at 400 °C.

2.2. Physicochemical characterization

The bulk composition was achieved at the Institute of Analytical Sciences (CNRS) using inductively coupled plasma atomic emission spectroscopy. Powder XRD analysis was performed on a Bruker AXS D8 advance diffractometer in Bragg-Brentano geometry fitted with a LynxEye Super Speed detector. Data were recorded with Cu K α radiation ($\lambda=0.154$ nm, 40 kV, 30 mA) on the 2 θ range 10–80° with a 2 θ step of 0.02°. The Fullprof Suite

program [25] was used for Rietveld refinement. H₂-Temperature-Programmed-Reduction (H₂-TPR) experiments were carried out on a Micromeritics AutoChem II 2920 apparatus with a constant heating rate of 5 °C min⁻¹. 50 mg of catalyst were exposed to a flow of 5 vol.% hydrogen diluted in argon. Specific Surface Areas (SSA) were calculated according to the BET method from nitrogen physisorption measurements at -196 °C on a Micromeritic Flow-sorb III. XPS experiments were performed on an AXIS Ultra DLD Kratos spectrometer equipped with a monochromatized aluminum source (150 W, $h\nu=1486.6$ eV) and a charge compensation gun or on a VG Scientific Escalab 220i-XL spectrometer equipped with a non-monochromatized aluminum source. All binding energies were referenced to the C1s core level at 285 eV. Semi-quantitative analysis took a linear background correction into account according to the procedure proposed by Shirley [26].

2.3. Catalytic activity measurements

Catalytic measurements were performed in a fixed bed flow reactor according to a standard procedure illustrated in Fig. 1. 200 mg of calcined catalysts in powder form (100–200 μ m) were mixed with SiC to avoid limitations related to heat and mass transfer phenomena. Prior to Temperature-Programmed-Reaction (TPR) experiments, the samples were heated in air at 600 °C. Four temperature cycles were performed in stoichiometric, lean, rich and finally stoichiometric conditions. The composition of the inlet mixtures are reported in Table 1. For sake of simplicity, only catalytic performances recorded in stoichiometric conditions during the first and last cycles, respectively labeled *Stoic 1* and *Stoic 2*, will be presented and discussed. Alternately the impact of oxygen content was investigated through the comparison of catalytic activities on Rh/La_{0.67}Fe_{0.83}Cu_{0.17}O₃ obtained during stoichiometric condition *Stoic 1* and *Stoic 2* and a modified stoichiometric condition *Modified stoic 1*. The global flow rate was 12 L h⁻¹ to insure a gas hourly space velocity of 60,000 mL h⁻¹ g⁻¹. Temperature-Programmed-Reaction (TPR) experiments were performed from 110 °C to 530 °C with a constant heating rate of 5 °C min⁻¹. The composition of the outlet gas mixtures was monitored by a chemiluminescence analyzer (ThermoFisher Scientific Mégatec Model 42i-HL) and an Agilent Technologies 490 micro GC. The activation energies were calculated from Arrhenius plots with low conversion levels. Rate constants (k) calculated from Eq. (1) were used where W stands for the mass of catalyst, Q_0 the total flow rate at the inlet of the reactor. The specific reaction rate was calculated according to Eq. (2). $F_{i,\text{inlet}}$ stands for the molar flow rate for i at the inlet of the reactor. Eq. (2) is established for a plug flow reactor and takes into account a first order kinetic reaction for CO or C₃H₆ oxidation.

$$k_i = \frac{Q_0}{W} \ln \left(\frac{1}{1 - X_i} \right) \quad (1)$$

$$r = k \frac{F_{i,\text{inlet}}(1 - X_i)Q_0}{(2)}$$

3. Results

3.1. Bulk properties

Main reflections on powder XRD patterns (Fig. 2) recorded on La_{1-y}Fe_{1-x}Cu_xO₃ appear at 2 θ ~ 22.6°, 32.2°, 39.8°, 46.2° and 57.6°. These XRD peaks characterize the typical orthorhombic structure of LaFeO₃ (JCPDS 37-1493). These structural features are conserved on lanthanum-deficient samples ($y=0.33$) and on samples with iron partly substituted by copper ($x=0.17$ and 0.2). No additional reflection ascribed to bulk segregation of α -Fe₂O₃ (JCPDS 73-2234) and CuO (JCPDS 48-1548) is detected. The use of the Rietveld refinement method for fitting structural parameters leads to optimized data

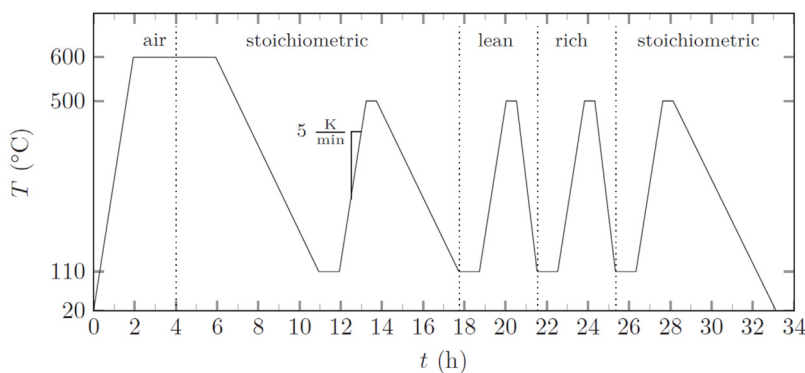


Fig. 1. Scheme of the experimental procedure for the evaluation of the catalytic performances.

Table 1

Typical composition of reaction mixtures and lambda values during TPR experiments under lean, rich and stoichiometric conditions.

Gas (vol.%)	NO	CO	CH ₄	C ₃ H ₆	C ₃ H ₈	H ₂	O ₂	CO ₂	H ₂ O	λ
Lean	0.1	0.5	0.0150	0.030	0.0150	0.167	0.935	15	10	0.978
Rich	0.1	0.9	0.0300	0.060	0.0300	0.300	0.609	15	10	1.018
Stoic 1/Stoic 2	0.1	0.7	0.0225	0.045	0.0225	0.233	0.777	15	10	0.999
Modified Stoic 1 ^a	0.1	0.7	0.0225	0.045	0.0225	0.233	0.732 ^a	15	10	1.001

^a Reduction of the relative concentration of oxygen corresponding to the fraction needed to convert methane.

Table 2

Structural properties of non-stoichiometry and partially substituted La_{1-y}Fe_xCu_{1-x}O₃ catalysts from XRD analysis.

Catalyst	a/Å	b/Å	c/Å	Unit cell Vol./Å ³	Cryst. size/nm	S _{th} ^a /m ² g ⁻¹
LaFeO ₃	5.561	7.858	5.558	242.85 ± 0.17	20.1 ± 0.1	45
La _{0.67} FeO ₃	5.556	7.851	5.558	242.43 ± 0.27	12.6 ± 0.1	71
LaFe _{0.8} Cu _{0.2} O ₃	5.559	7.829	5.548	241.46 ± 0.22	13.5 ± 0.1	67
La _{0.67} Fe _{0.83} Cu _{0.17} O ₃	5.564	7.833	5.558	242.43 ± 0.26	13.3 ± 0.1	68

^a Calculated from the crystallite size of LaFeO₃ obtained from XRD with S_{th} = 6.10³/(ρ·d_{crystallite}).

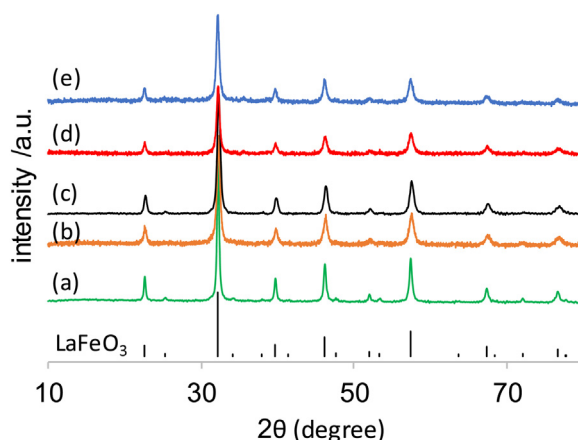


Fig. 2. XRD patterns recorded on calcined LaFeO₃ (a), La_{0.67}FeO₃ (b), LaFe_{0.8}Cu_{0.2}O₃ (c), La_{0.67}Fe_{0.83}Cu_{0.17}O₃ (d), 0.1 wt.%Rh/La_{0.67}Fe_{0.83}Cu_{0.17}O₃ (e) and LaFeO₃ reference (00-037-1493).

collected in **Table 2**. La-deficient La_{0.67}FeO₃ exhibits comparable structural parameters to those adjusted on stoichiometric LaFeO₃ perovskite. Both structures have a similar cell volume with values varying within the margin of error. Copper substitution induces a lattice contraction only for stoichiometric LaFe_{0.83}Cu_{0.17}O₃ solid which could be related to the stabilization of Fe⁴⁺ ions, characterized by a lower ionic radius (0.585 Å instead of 0.645 Å for Fe³⁺) or a stabilization of oxygen defects. Interestingly, the reverse trend is observed on La_{0.67}Fe_{0.83}Cu_{0.17}O₃, with a volume expansion which may suggest that the most stable oxidation state of iron (III) could

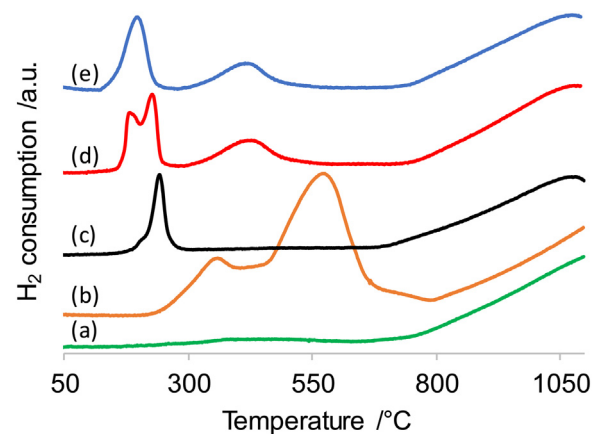


Fig. 3. H₂-TPR experiments performed on calcined LaFeO₃ (a), La_{0.67}FeO₃ (b), LaFe_{0.8}Cu_{0.2}O₃ (c), La_{0.67}Fe_{0.83}Cu_{0.17}O₃ (d), 0.1 wt.%Rh/La_{0.67}Fe_{0.83}Cu_{0.17}O₃ (e).

be restored to compensate La-deficiency and insure the electrical neutrality.

The crystallite size calculated from the Rietveld method decreases on La-deficient samples and on LaFe_{0.8}Cu_{0.2}O₃ as compared to the initial LaFeO₃ solid.

The bulk reducibility of the solids was investigated by H₂-Temperature-Programmed-Reduction experiments (H₂-TPR). The profiles of H₂ consumption curves vs. temperature are compared in **Fig. 3**. No significant reduction process takes place on LaFeO₃ below 700°C. A broad signal appears in the temperature range 300–600°C only for La-deficient lanthanum perovskite samples which has been previously ascribed to the two-step reduction of

segregated hematite (α -Fe₂O₃) [9]. An additional signal appears on Cu-substituted samples below 300 °C with no significant overlapping with the reduction process ascribed to oxidic iron species.

A single reduction peak is discernible for the reduction of copper species on LaFe_{0.2}Cu_{0.8}O₃ and Rh/La_{0.67}Fe_{0.83}Cu_{0.17}O₃ whereas two components characterize the overall signal recorded on La_{0.67}Fe_{0.83}Cu_{0.17}O₃ with maximum temperature at 182 and 227 °C (Table 3). Such an observation may be explained either by a two-step reduction process of either a single Cu²⁺ species involving the intermediate production of Cu⁺ or by the existence of two distinct Cu²⁺ species stabilized in different chemical environments.

The reduction of oxidic iron species is not observed on stoichiometric solids below 700 °C. We can therefore rule out the possible stabilization of Fe⁴⁺ and/or the contribution of segregated iron oxides clusters due to iron substitution by copper. On the other hand, the broad H₂ consumption is recorded on La_{0.67}FeO₃, La_{0.67}Fe_{0.87}Cu_{0.13}O₃ and 0.1 wt. Rh/La_{0.67}Fe_{0.87}Cu_{0.13}O₃ solids which suggest that iron oxide species can coexist with perovskite structure.

It is remarkable that Rh incorporation to La_{0.67}Fe_{0.83}Cu_{0.17}O₃ speeds up the complete reduction of copper species into metallic Cu⁰. An estimate of the atomic H/Cu and H/Fe ratios is proposed in Table 3 from H₂-TPR experiments. A complete reduction of oxidic copper species does not occur on LaFe_{0.8}Cu_{0.2}O₃ compared to La_{0.67}Fe_{0.83}Cu_{0.17}O₃ and Rh/La_{0.67}Fe_{0.83}Cu_{0.17}O₃ solids. The surface composition can perhaps influence the reducibility of perovskite-based catalysts.

3.2. Surface properties

Perovskite-based catalysts usually have low specific surface area around 10–20 m²/g when conventional citrate method is used [27]. Significant enhancement on the specific surface area is noticeable on La-deficient La_{0.67}FeO₃ and La_{0.67}Fe_{0.83}Cu_{0.17}O₃ samples compared to the parents LaFeO₃ and LaFe_{0.8}Cu_{0.2}O₃. This trend seems in good agreement with the formation of smaller crystallites estimated by XRD analysis. The ratio between the surface area calculated from crystallite size (Table 2) and the surface measured by BET method is between 2.6 and 4.8. This comparison suggests the creation of porosity via the agglomeration of individual particles and is in agreement with previous investigation [22,28].

Surface properties (oxidation state, surface concentration) were investigated with X-ray Photoelectron Spectroscopy. XPS photo-peaks for Fe2p, Cu2p, O1s and C1s core levels are illustrated in Fig. 4(A)–(D). Spectral features, i.e. binding energy (B.E.) values and relative concentrations, are summarized in Table 4. No significant change is noticeable on the La 3d_{5/2} B.E. characteristic of La³⁺ species (not shown). The B.E. values for Fe2p_{3/2} photopeak and the observation of a shake-up satellite structure at 719 eV highlight the stabilization of Fe³⁺ species. The Cu2p_{3/2} photopeak centered at 933 eV is accompanied by the presence of a shake-up satellite structure in the range 939–947 eV which reflects the presence of Cu²⁺. It should be mentioned that the reduction of Cu²⁺ species into Cu⁺/Cu⁰ can occur under vacuum and irradiation with X-ray source [29]. The intensity of the shake-up satellite structure strongly attenuates on La_{0.67}Fe_{0.83}Cu_{0.17}O₃ solid when longer accumulation time is used (spectra not shown). Therefore we choose to present Cu2p spectra recorded with short accumulation time despite the lower signal to noise ratio (spectra (d) and (e)). The high sensibility of copper species towards vacuum and/or irradiation with X-ray source can be related to the higher reducibility of copper species observed during H₂-TPR experiments on La_{0.67}Fe_{0.83}Cu_{0.17}O₃ and Rh/La_{0.67}Fe_{0.83}Cu_{0.17}O₃ solids. On the other hand the Cu2p 3/2 photopeak is broader on LaFe_{0.8}Cu_{0.2}O₃ solid than on La_{0.67}Fe_{0.83}Cu_{0.17}O₃ and Rh/La_{0.67}Fe_{0.83}Cu_{0.17}O₃ solids. A spectral decomposition of Cu 2p photopeak suggests the

presence of an additional signal at high B.E. values in parallel with the main component at 933.3 eV previously assigned to Cu²⁺ in the perovskite. The formation of Cu(OH)₂ species was previously proposed by Biesinger et al. can be in good agreement with the B.E. 934.6 eV observed in the decomposition [30].

Regarding the O1s photopeak, two contributions arise on the overall signal. The predominant component in the B.E. range 528.9–530.0 eV is currently ascribed to lattice oxygen O²⁻ from the perovskite whereas the shoulder at higher B.E. value corresponds to adsorbed O species such as O⁻, O²⁻ or OH⁻ [31]. Let us note that a growth in intensity of this latter contribution is usually associated with the stabilization of carbonates as evidenced on the C1s photopeak around 289 eV.

The surface concentrations are summarized in Table 4. The main information comes from the surface atomic ratio La/(Fe + Cu). The objective of our study was to decrease the lanthanum excess at the surface thanks to the lanthanum-deficient synthesis [9,22]. On one hand, the stoichiometric LaFeO₃ and LaFe_{0.8}Cu_{0.2}O₃ samples have a typical value of La/(Fe + Cu) above 1.8. On the other hand the La-deficient samples have much lower values between 0.88 and 1.03, which is in line with the theoretical value of ideal perovskite structures. The presence of Lanthanum excess at the surface can be related to a lower H₂ consumption observed on stoichiometric samples during H₂-TPR on the series of LaFeO₃ and LaFeCuO₃ solids.

3.3. Catalytic measurements

3.3.1. On calcined catalysts

Impact of partial substitution of Fe by Cu, Lanthanum-deficient synthesis and Rhodium doping on the catalytic activity in TWC was investigated. As mentioned earlier, the discussion will be restricted to catalytic data obtained in stoichiometric conditions during the first and the last temperature cycles as described in Fig. 1.

Temperature-programmed conversion curves for CO, C₃H₆ and NO during *Stoic 1* and *Stoic 2* conditions are reported in Fig. 5. Prior to catalytic measurements all samples were systematically treated in air at 600 °C. Catalytic data are compared to those obtained on a reference commercial catalyst containing Pd and Rh metals. First, the conversion of NO is only activated on Rh-doped perovskite sample during the *Stoic 2* sequence. The conversion of NO is almost nil during *Stoic 1* and *Stoic 2* cycles on La_{1-y}Fe_{1-x}Cu_xO₃ catalysts with y = 0, 0.33 and x = 0.2, 0.17. On the other hand, a partial substitution of iron by copper coupled with lanthanum-deficient synthesis leads to remarkable improvements in CO conversion especially on La_{0.67}Fe_{0.87}Cu_{0.13}O₃.

Subsequent incorporation of 0.1 wt.% Rh to La_{0.67}Fe_{0.87}Cu_{0.13}O₃ has no significant effect on conversion level during the *Stoic 1* cycle. Indeed, the conversion of NO remains almost nil. Slightly lower conversion in CO and C₃H₆ are observable surprisingly and this highlights the poor activity of rhodium for oxidation reaction on calcined catalyst. On the other hand, the *Stoic 2* temperature cycle reveals significant improvements to CO and propene oxidation as well as to NO reduction on 0.1 wt.% Rh/La_{0.67}Fe_{0.87}Cu_{0.13}O₃ catalyst. The comparison of *Stoic 1* and *Stoic 2* gives additional information concerning the stability of the solid.

Catalytic features can be discussed in terms of temperature at half-conversion (T₅₀), specific and intrinsic reaction rates, apparent activation energy values and pre-exponential factor values (Table 5). A shift of T₅₀ for CO oxidation from 438 °C to 232 °C on LaFeO₃ and La_{0.67}Fe_{0.87}Cu_{0.13}O₃ respectively highlights the effect of partial substitution of iron by copper and the lanthanum-deficient synthesis. This effect is accompanied with a sharp decrease in the apparent activation energy from 142 to 59 kJ mol⁻¹ for CO oxidation on LaFeO₃ and La_{0.67}Fe_{0.87}Cu_{0.13}O₃ respectively. Propene oxidation is also enhanced but to a lower extent with T₅₀ decreasing from 463 °C to 386 °C on LaFeO₃ and La_{0.67}Fe_{0.87}Cu_{0.13}O₃ respec-

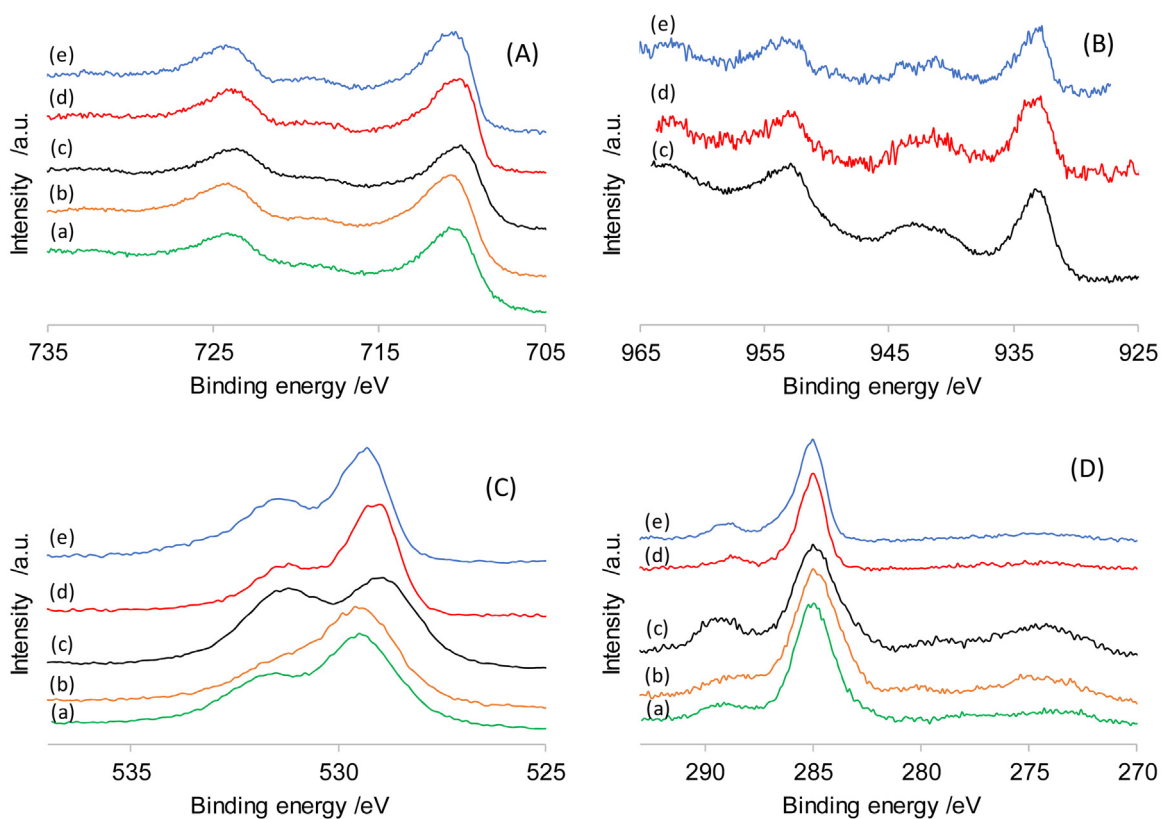


Fig. 4. XPS spectra recorded on calcined LaFeO_3 (a), $\text{La}_{0.67}\text{FeO}_3$ (b), $\text{LaFe}_{0.8}\text{Cu}_{0.2}\text{O}_3$ (c), $\text{La}_{0.67}\text{Fe}_{0.83}\text{Cu}_{0.17}\text{O}_3$ (d), 0.1 wt.%Rh/ $\text{La}_{0.67}\text{Fe}_{0.83}\text{Cu}_{0.17}\text{O}_3$ (e) – Fe 2p photopeak (A), Cu 2p photopeak (B), O 1s photopeak (C) and C 1s photopeak (D).

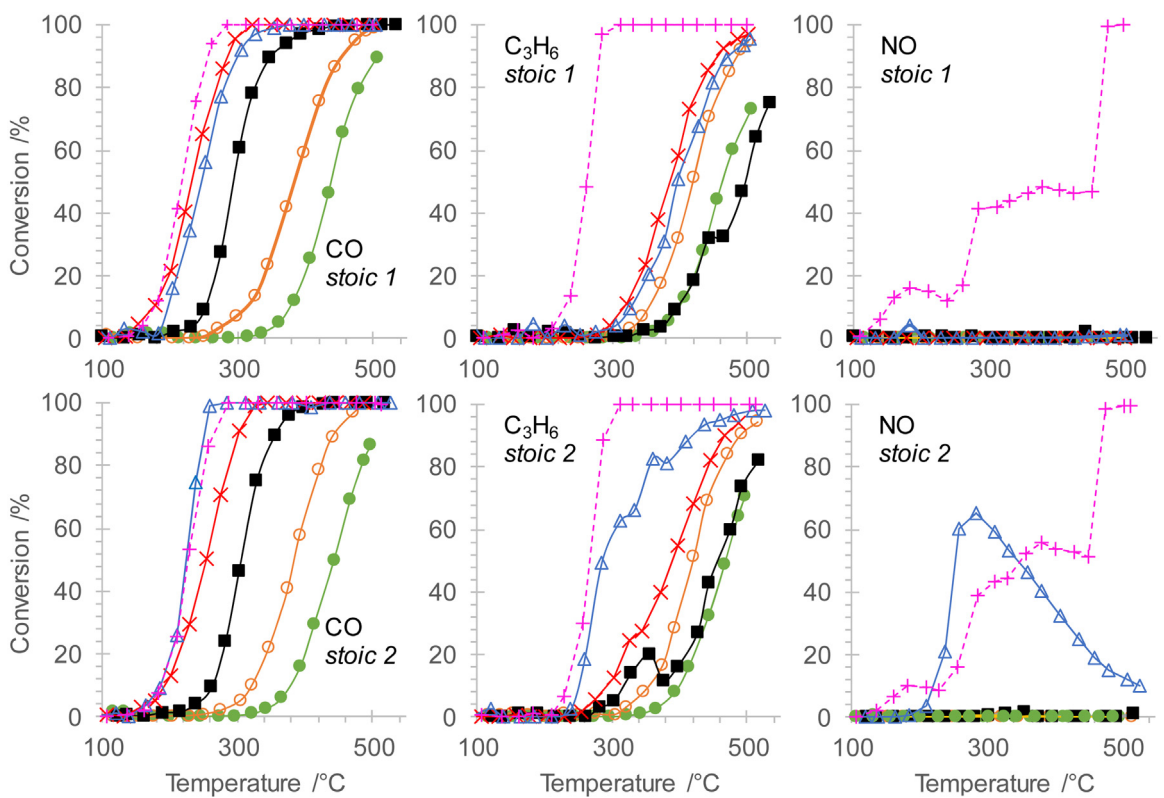


Fig. 5. Temperature-Programmed conversion curves recorded during stoic 1 and stoic 2 cycle on calcined LaFeO_3 (●), $\text{La}_{0.67}\text{FeO}_3$ (○), $\text{LaFe}_{0.8}\text{Cu}_{0.2}\text{O}_3$ (■), $\text{La}_{0.67}\text{Fe}_{0.83}\text{Cu}_{0.17}\text{O}_3$ (✗), 0.1 wt.%Rh/ $\text{La}_{0.67}\text{Fe}_{0.83}\text{Cu}_{0.17}\text{O}_3$ (△) and the commercial TWC reference (+).

Table 3

Reducibility of perovskite-based catalysts: Influence of lanthanum sub-stoichiometry and rhodium incorporation.

Catalyst	Spec. surf. area/m ² g ⁻¹	H ₂ uptake/mmol g ⁻¹	T _{Max} /°C		H/Cu		H/Fe	
			Low T ^a	High T ^a	Low T ^a	High T ^a	Low T ^a	High T ^a
LaFeO ₃	13.9	n.d ^b	n.d ^b	n.d ^b	–	–	–	–
La _{0.67} FeO ₃	21.5	1.83	–	571	–	–	0.72	
LaFe _{0.8} Cu _{0.2} O ₃	13.8	0.67	241	n.d ^b	1.64		–	
La _{0.67} Fe _{0.83} Cu _{0.17} O ₃	26.5	1.76	182, 227	422	2.33	0.36		
Rh/La _{0.67} Fe _{0.83} Cu _{0.17} O ₃	27.5	1.79	196	417	2.28	0.38		

^a Low T: 50–~300 °C; High T: ~300–700 °C.^b No detection.**Table 4**XPS analysis of stoichiometric and La-deficient LaFeO₃-based perovskites.

Catalyst	B.E. (eV)				Relative Surface Atomic Composition					
	La 3d _{5/2}	Fe 2p _{3/2}	Cu 2p _{3/2}	O1s	La/Fe + Cu	Cu/Fe	O/Total ^a	C/Total ^a	O _{lattice}	O _{ads}
LaFeO ₃	834.3	710.8	–	529.5	2.13	–	0.44	0.35	0.55	0.45
La _{0.67} FeO ₃	834.3	710.4	–	529.6	0.88	–	0.53	0.32	0.34	0.66
LaFe _{0.8} Cu _{0.2} O ₃	833.9	710.1	933.2	528.9	1.82	0.35	0.46	0.27	0.46	0.53
La _{0.67} Fe _{0.83} Cu _{0.17} O ₃	834.5	710.9	933.1	530.0	1.03	0.22	0.41	0.25	0.65	0.35
Rh/La _{0.67} Fe _{0.83} Cu _{0.17} O ₃	834.1	710.4	932.7	529.3	1.00	0.12	0.39	0.35	0.43	0.57

^a Total = La + Fe + Cu + C + O.**Table 5**Kinetic features on stoichiometric and La-deficient LaFeO₃-based perovskites obtained in stoichiometric conditions.

Catalyst	TPR cycle	Temperature at Half Conv. (°C)			r _{specific} (mols ⁻¹ g ⁻¹)		r _{intrinsic} (mol s ⁻¹ m ⁻²)		E _{A,app} (kJ mol ⁻¹)		A (m ³ s ⁻¹ g ⁻¹)	
		CO	C ₃ H ₆	C ₃ H ₈	CO/×10 ⁻⁷ ^a	C ₃ H ₆ /×10 ⁻⁹ ^b	CO/×10 ⁻⁹ ^a	C ₃ H ₆ /×10 ⁻¹⁰ ^b	CO	C ₃ H ₆	CO	C ₃ H ₆
LaFeO ₃	Stoic1	438	463	478	~0	5.2	~0	3.8	142	134	4.2.10 ⁵	4.6.10 ⁴
	Stoic2	443	468	481	~0	4.9	~0	3.5	129	140	3.5.10 ⁴	1.2.10 ⁵
La _{0.67} FeO ₃	Stoic1	384	420	497	~0	26	~0	12	79	119	20	1.3.10 ⁴
	Stoic2	384	420	484	~0	26	~0	12	99	105	840	903
LaFe _{0.8} Cu _{0.2} O ₃	Stoic1	294	497	>500	0.9	7.7	6.2	5.6	84	108	408	426
	Stoic2	306	455	>500	0.7	51	4.9	37	70	69	12	0.7
La _{0.67} Fe _{0.87} Cu _{0.13} O ₃	Stoic1	232	386	>500	8.6	66	33	25	59	124	12	1.5.10 ⁵
	Stoic2	255	390	>500	3.2	76	12	29	60	106	10	8.6.10 ³
Rh/La _{0.67} Fe _{0.87} Cu _{0.13} O ₃	Stoic1	247	397	493	5.7	52	21	19	67	89	69	106
	Stoic2	225	286	471	7.8	105	28	38	75	169	607	8.7.10 ¹⁰
Reduced Rh/La _{0.67} Fe _{0.87} Cu _{0.13} O ₃	Stoic1 ^c	218	287	464	9.5	100	38	40	105	115	1.8.10 ⁶	5.6.10 ⁵
	Stoic2 ^c	223	269	469	8.4	77	34	31	120	266	6.2.10 ⁷	6.6.10 ²⁰
Reduced Rh/La _{0.67} Fe _{0.87} Cu _{0.13} O ₃	Mod. Stoic1	217	305	457	12	112	42	41	70	167	263	3.7.10 ¹⁰
	Mod. Stoic2	222	285	471	8.8	108	32	39	67	145	100	5.4.10 ⁸
Commercial PGM catalyst	Stoic2	217	262	455	n.c.	n.c.	n.c.	n.c.	n.c.	n.c.	n.c.	n.c.
	Stoic2	228	268	457	n.c.	n.c.	n.c.	n.c.	n.c.	n.c.	n.c.	n.c.

^a T(reaction) = 200 °C for CO oxidation by oxygen.^b T(reaction) = 350 °C for propene oxidation by oxygen.^c The treatment in air at 600 °C was replaced by a reductive treatment in 5% H₂ in He at 300 °C.

tively. As observed there is no noticeable fluctuation of the T₅₀ values recorded during Stoic1 and Stoic2 temperature cycle, this reflects a relatively stable surface and stable perovskite structure on this series of catalysts. The comparison of the T₅₀ values with those measured on the commercial catalyst suggests at this stage that La_{0.67}Fe_{0.87}Cu_{0.13}O₃ can compete for oxidation reactions. The La_{0.67}Fe_{0.87}Cu_{0.13}O₃ catalyst could be an excellent substitute to palladium/rhodium which is usually involved in the CO/O₂ oxidation and oxidation of unburnt hydrocarbons.

Significant improvements on Rh/La_{0.67}Fe_{0.87}Cu_{0.13}O₃ catalyst are observed for the conversion of propene and to a lower extent for CO conversion between the Stoic1 and Stoic2 sequence. A sharp decrease of the T₅₀ for propene oxidation from 397 °C to 286 °C is observed and to a lower extent for CO oxidation. Similar conversion levels are obtained on the commercial catalysts and on Rh/La_{0.67}Fe_{0.87}Cu_{0.13}O₃ catalyst during the Stoic2

cycle. Both specific reaction rates and intrinsic reaction rates for CO and propene oxidation increase between the Stoic1 and Stoic2 sequence which suggests a change in the nature of active site on Rh/La_{0.67}Fe_{0.87}Cu_{0.13}O₃ catalyst. An activation of Rh/La_{0.67}Fe_{0.87}Cu_{0.13}O₃ takes place during the cycle and reflects either structural changes related to rhodium re-dispersion at the surface of the perovskite or a change in the oxidation state of rhodium. Indeed, in the absence of precious metal, the catalytic performances of the perovskites are maintained irrespective of La-deficiency and degree of partial substitution of iron by copper.

3.3.2. On pre-reduced catalysts

The nature of pre-treatment and the influence of oxygen concentration during experiment will be investigated in the following section on Rh/La_{0.67}Fe_{0.87}Cu_{0.13}O₃ catalyst. Based on previous observations, Rh/La_{0.67}Fe_{0.87}Cu_{0.13}O₃ catalyst was pre-activated in

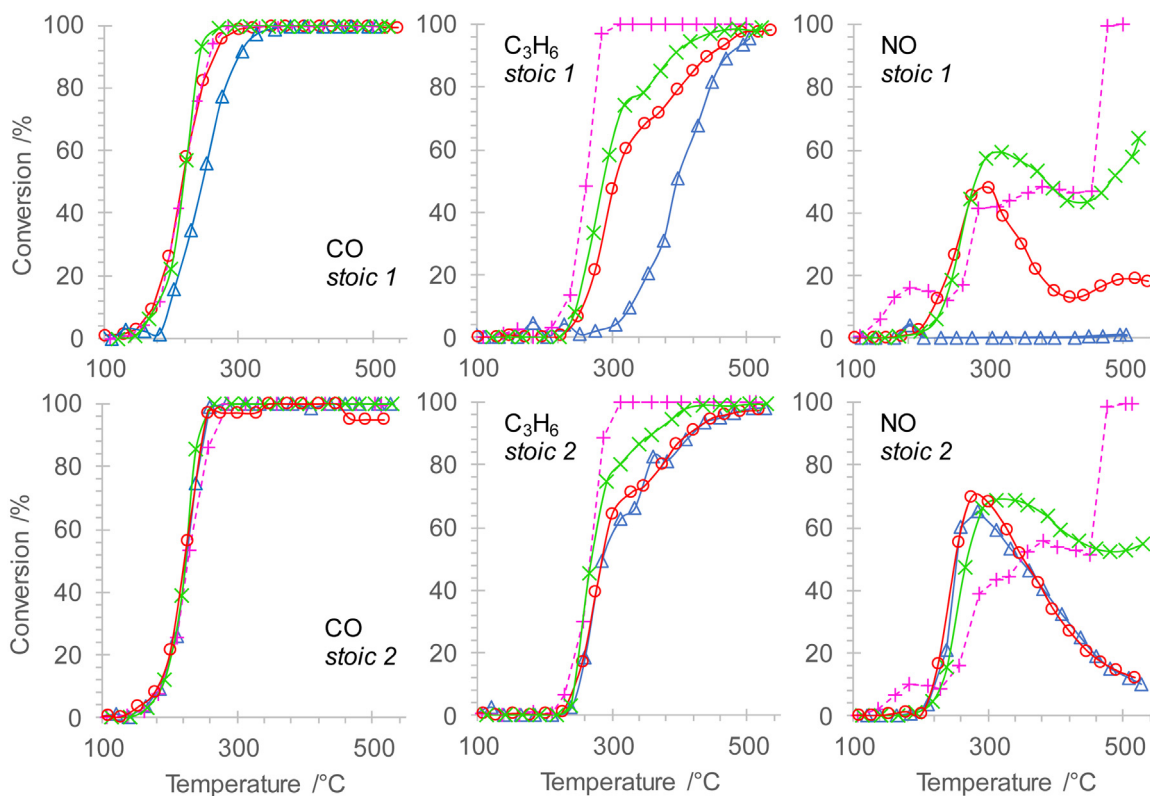


Fig. 6. Temperature-Programmed conversion curves recorded during stoic 1 and stoic 2 cycles on calcined 0.1 wt.%Rh/La_{0.67}Fe_{0.83}Cu_{0.17}O₃ (Δ), on pre-reduced 0.1 wt.%Rh/La_{0.67}Fe_{0.83}Cu_{0.17}O₃ (\circ), on the commercial TWC reference (+) and during Modified stoic 1 and Modified stoic 2 cycle on pre-reduced 0.1 wt.%Rh/La_{0.67}Fe_{0.83}Cu_{0.17}O₃ (x).

5 vol.% H₂ diluted in helium at 300 °C for 5 h prior to temperature-programmed reaction experiments. The commercial catalyst was also submitted to the same thermal pre-treatment. The major change observed in Fig. 6 is related to the sharp gain in NO conversion during the first Stoic1 temperature cycle. Significant improvements are also observed for the conversion of propene. Interestingly, Rh/La_{0.67}Fe_{0.87}Cu_{0.13}O₃ converges to similar conversion level for propene during the Stoic1 temperature cycle whatever the nature of the pre-treatment. This suggests the stabilization of comparable surface properties despite different pre-activation thermal treatment. Another point concerns the stability of catalytic activity. For example the NO conversion is even higher during the second Stoic2 cycle than during the Stoic1 cycle. This increase of conversion can be related to the metallic oxidation state of rhodium particles even in stoichiometric conditions.

It should be mentioned that the reaction mixture is composed of 225 ppm CH₄ in Stoic1 and Stoic2. Methane conversion is quite difficult below 450 °C. We have slightly modified the composition of the reaction composition by reducing the oxygen content for Modified Stoic1 composition (Table 1). In those conditions, further improvement on the conversion of NO and propene is noticeable on Modified Stoic1 and Modified Stoic2.

Another interesting point concerns the selectivity and yield in N₂, N₂O and NH₃ observed during NO reduction. On calcined Rh/La_{0.67}Fe_{0.87}Cu_{0.13}O₃ catalyst, the NO conversion increases above 150 °C up a maximum of 62% at 282 °C during Stoic2 cycle. The yield in N₂, N₂O and NH₃ is presented in Fig. 7 for Rh/La_{0.67}Fe_{0.87}Cu_{0.13}O₃ catalyst with regards to the nature of the activation (calcination, reduction...).

Nitrous oxide and nitrogen are mainly formed on Rh/La_{0.67}Fe_{0.87}Cu_{0.13}O₃ catalyst. The yield of N₂O increases until 280–300 °C then gradually decreases and becomes almost

nil at 530 °C on Rh/La_{0.67}Fe_{0.87}Cu_{0.13}O₃ catalyst whatever the thermal pre-treatment. The yield in nitrogen is higher on Rh/La_{0.67}Fe_{0.87}Cu_{0.13}O₃ catalyst than on commercial TWC below 370 °C and 400 °C on Stoic1 and Stoic2 respectively. Another difference between the commercial reference and the Rh/La_{0.67}Fe_{0.87}Cu_{0.13}O₃ catalyst concerns the production of ammonia at high temperature.

A low yield in ammonia (below 8% in all cases) on Rh/La_{0.67}Fe_{0.87}Cu_{0.13}O₃ is measured on Stoic1 and Stoic2 whereas it exceeds 60% on the commercial catalyst at 500 °C.

It may be highlighted that the conversion of propane increases at the same time as a subsequent production of H₂ is observed (above ~450 °C). The production of hydrogen from propane reforming can be related to the formation of ammonia on the commercial reference. On the other hand the lower production of ammonia observed on Rh/La_{0.67}Fe_{0.87}Cu_{0.13}O₃ suggests that reforming reactions are slowed down on Rh/La_{0.67}Fe_{0.87}Cu_{0.13}O₃. The high catalytic activity for CO and unburnt hydrocarbons oxidation into CO₂ and H₂O can limit the occurrence of reforming reactions which produce hydrogen responsible of the formation of ammonia.

The decrease of oxygen content during Modified stoic1 and Modified stoic2 has no influence on N₂O yield for Rh/La_{0.67}Fe_{0.87}Cu_{0.13}O₃ catalyst. The yield in nitrogen significantly increases above 300 °C. Similarly the yield of ammonia increases during Modified stoic1 and Modified stoic2 but remains below 20% on Rh/La_{0.67}Fe_{0.87}Cu_{0.13}O₃ catalyst.

4. Discussion

A continuous effort is made to improve the catalytic properties of perovskite-type oxides in automotive applications since the work of Voorhoeve et al. [32]. This study is devoted to the develop-

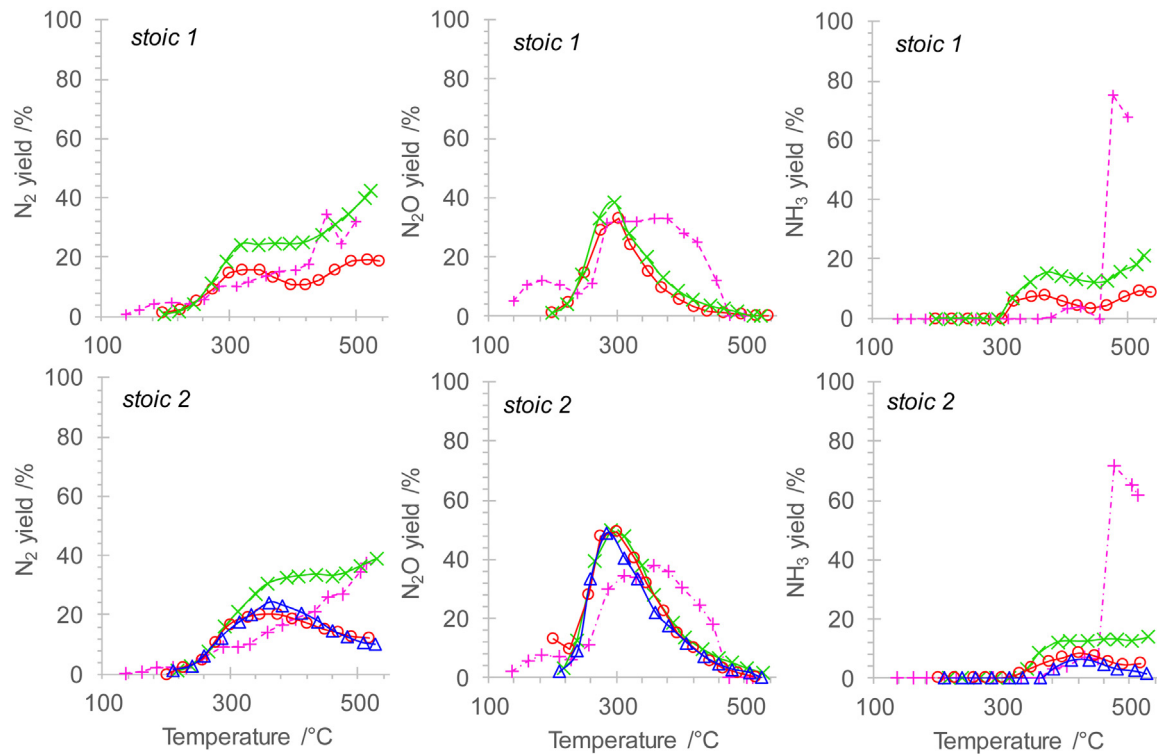


Fig. 7. Product distribution profiles from Temperature-Programmed NO reduction experiments during stoic 1 and stoic 2 cycle on calcined 0.1 wt.%Rh/La_{0.67}Fe_{0.83}Cu_{0.17}O₃ (Δ), on pre-reduced 0.1 wt.%Rh/La_{0.67}Fe_{0.83}Cu_{0.17}O₃ (○), on the commercial TWC reference (+) and during Modified stoic 1 and Modified stoic 2 cycle on pre-reduced 0.1 wt.%Rh/La_{0.67}Fe_{0.83}Cu_{0.17}O₃ (×).

ment of Rh-doped La_{1-y}Fe_{1-x}Cu_xO₃ catalysts for three-way catalysis and clearly puts into evidence cooperative effects of the perovskite structure with low content of Rh (0.1 wt.%) dispersed at the surface, the former one being more active for the catalytic oxidation of CO, propene and propane whereas rhodium is active essentially for the reduction of NO to nitrogen. Two strategies lead to significant improvement of catalytic performances: copper insertion into the perovskite lattice and the optimization of surface composition thanks to lanthanum-deficient synthesis.

One of the advantages of perovskite structures exploited in this study is the ability to accommodate different stoichiometry and different oxidation state by varying the stoichiometry of lanthanum and the nature of the B site through partial substitution of iron by copper. The partial substitution of trivalent lanthanum cations by lower valence state elements generally leads to modification of the valence state of the B-site and/or the creation of lattice oxygen vacancies for maintaining the electrical neutrality [33,34]. In the particular case of La-deficient perovskite samples, the lanthanum deficiency could also induce the creation of oxygen vacancies and partial reduction of the B-sites than improving the oxygen mobility as reported elsewhere [33,34]. Otherwise, partial extraction of iron and/or copper at the surface can also create anionic vacancies [33,34].

H₂-TPR experiments provide interesting observations. The broad H₂ uptakes recorded on La_{0.67}FeO₃, La_{0.67}Fe_{0.87}Cu_{0.13}O₃ and Rh/La_{0.67}Fe_{0.87}Cu_{0.13}O₃ suggest that both iron species could coexist. On copper-substituted samples, a low consumption process ascribes to the reduction of oxidic copper species occurs at low temperature more readily on Rh-doped perovskite. It seems consistent with previous findings demonstrating a higher reducibility of the perovskite surface when noble metal are dispersed at the surface rather than stabilized inside the perovskite structure [16]. The use of low Rh loadings considerably limits their detection and

quantification from XPS analysis according to the degree of dispersion. The higher Rh dispersion on La-deficient perovskite sample has not been formally related to changes in specific surface area but more likely to the extent of interaction between cationic Rh species and anionic vacancies favoring re-dispersion process at the surface [35]. Such an explanation is consistent with previous DFT calculations concluding that without oxygen vacancy the tendency of palladium to migrate from the bulk and segregate at the surface would be weak.

The formation of anionic vacancies has positive effect since NO can adsorb and dissociate more readily on anionic vacancies [36]. It is also noticeable that oxygen defects can also enhance the molecular adsorption of oxygen [37] which seems consistent with the significant rate enhancement on the rate of CO oxidation by O₂ on La_{0.67}Fe_{0.83}Cu_{0.17}O₃ compared to La_{0.67}FeO₃.

With regards to the CO/O₂ reaction, Table 5 shows that partial substitution of copper has a beneficial effect on the catalytic activity much more pronounced on the sub-stoichiometric La_{0.67}Fe_{0.83}Cu_{0.17}O₃ sample than on LaFe_{0.8}Cu_{0.2}O₃. Parallel to a sharp increase in specific rate, the lowering of apparent activation energy reflects better intrinsic properties. It is noticeable that subsequent incorporation of Rh has no significant effect during Stoic1 cycle emphasizing the fact that their performances are intimately related to the surface stoichiometry of perovskite. Improvement in catalytic performance of La_{0.67}Fe_{0.83}Cu_{0.17}O₃ compared to LaFe_{0.8}Cu_{0.2}O₃ illustrated by lower activation energies likely reflect the ease of oxygen removal from the lattice or stabilized as adsorbates [38]. However, it is worth to note that the CO/O₂ reaction occurs at rather low temperature on our solids which could suggest that the participation of gaseous oxygen molecule chemisorbed on surface anionic vacancies could be more relevant in agreement with significant improvement of the reducibility of La_{0.67}Fe_{0.83}Cu_{0.17}O₃ compared to LaFe_{0.8}Cu_{0.2}O₃. However, the

involvement of mixed valence state for copper (Cu^{2+} , Cu^{3+}) [39] as well as self-regenerative behavior leading to possible partial extraction of copper species cannot be totally rule out. As a matter of fact, this latter explanation seems more in agreement with H_2 -TPR experiments with a reduction process for oxidic copper species taking place more readily on $\text{La}_{0.67}\text{Fe}_{0.83}\text{Cu}_{0.17}\text{O}_3$ and correlatively the disappearance of the shake-up structure characteristic of Cu^{2+} as previously discussed.

Significant evolutions of the catalytic properties affect Rh-doped perovskite catalysts pre-activated in air or hydrogen suggesting an equilibration of the oxidation state of rhodium as well as the accommodation of a greater extent of anionic vacancies providing better oxygen storage properties. This assumption could be supported by the observation of better catalytic properties and greater stabilization when the catalyst is preliminary reduced. Summarizing the most important trends it seems obvious that the concentration of defective sites can play a crucial role because oxygen adsorption can be promoted with a rise in concentration of surface lattice oxygen especially at increasing temperature as earlier found [40]. Our observations seem consistent with this finding showing a marked enhancement of CO and propane (not shown) oxidation on La-deficient and Cu-substituted perovskite samples.

Finally, it is worth to note that propene oxidation provides an excellent example consisting in comparing the specific surface area and the intrinsic rate on promoted and non-promoted $\text{La}_{0.67}\text{Fe}_{0.83}\text{Cu}_{0.17}\text{O}_3$ by Rh addition. As exemplified in Table 5, intrinsic rates recorded during *Stoic1* and *Stoic2* cycle increase which could suggest that Rh can drive directly or indirectly the conversion of propene. A sharp increase in the specific rate is also observable from *Stoic1* and *Stoic2* cycle which can reflect equally an increase in the density of active sites and in the composition of active sites. Hence, Rh species could act as active species and/or assist the creation of more active defective sites demonstrating the complexity of such surface.

The practical use of perovskite suffers from significant drawbacks associated with the thermal resistance to sintering and the sulfur tolerance. The thermal resistance of our solids is investigated through the specific procedure described in Fig. 1. The catalyst is first stabilized at 600 °C in presence of H_2O and the catalytic performances are measured successively in stoichiometric, lean, rich and stoichiometric conditions from 110 °C to 530 °C. The comparison of initial and last cycle measured in stoichiometric conditions provides a direct indication about the thermal resistance. This trend demonstrates the stability of our solids in presence of steam. During practical application in TWC, it is expected that stability under different reducing and oxidizing condition are assured, even at high temperature. The H_2 -TPR profile of LaFeO_3 indicates that the reduction in 5%vol. H_2 starts above 700 °C and underlines the stabilization of perovskite structure. On the other hand, the stability in rich condition could not be obtained on La_2CuO_4 [21]. The stabilization of perovskite structure by iron is also demonstrated in the case of $\text{LaFe}_{0.65}\text{Co}_{0.325}\text{Pd}_{0.025}\text{O}_3$ whereas the complete reduction of LaCoO_3 proceeds at low temperature in hydrogen [41,42].

The potential use of perovskite for automotive application can be limited by the deactivation by sulfur. The impact of sulfur over NO_x conversion is reported by Kim et al. on $\text{La}_{0.9}\text{Sr}_{0.1}\text{MnO}_3$ [6]. They demonstrate that a desulfation process performed at 700 °C can restore almost initial activity.

The thermal stability in different reducing/oxidizing atmosphere and the catalytic performances of 0.1wt%Rh/ $\text{La}_{0.67}\text{Fe}_{0.87}\text{Cu}_{0.13}\text{O}_3$ suggest further developments in TWC as one of the wash-coat layer in order to enable further reductions in precious metal use.

5. Conclusion

This study is devoted to the development of Rh-doped $\text{La}_{1-y}\text{Fe}_{1-x}\text{Cu}_x\text{O}_3$ catalysts for three-way catalysis. The orthorhombic structure of perovskite is obtained for all solids even in the case of Lanthanum-deficient synthesis. The surface analysis confirms that the decrease in lanthanum content in the bulk can decrease the typical lanthanum excess observed at the surface of lanthanum-based perovskite. The perovskite structure becomes more active for the catalytic oxidation of CO and propene by the combination of Lanthanum-deficient synthesis and partial substitution of iron by copper. The further addition of metallic rhodium particles develops the catalytic activity in the reduction of NO. The catalytic activity of these Rh-doped $\text{La}_{1-y}\text{Fe}_{1-x}\text{Cu}_x\text{O}_3$ catalysts is stable even after several cycles in stoichiometric, rich, lean conditions. The conversion levels for CO, unburnt hydrocarbons and NO pollutants in stoichiometric conditions are significantly enhanced on Rh/ $\text{La}_{0.67}\text{Fe}_{0.83}\text{Cu}_{0.17}\text{O}_3$ and this catalyst can be an interesting alternative to conventional three-way catalyst.

Acknowledgements

We would like to thank the European Union for the funding received within the FP7 research project under the grant agreement N°280890-NEXT-GEN-CAT and the Région Nord-Pas-de-Calais through the «Institut de Recherche en ENvironnement Industriel (IRENI)». We gratefully acknowledge the «Fonds Européen de Développement Régional (FEDER)», the CNRS, the Région Nord Pas-de-Calais and the «Ministère de l'Education Nationale de l'Enseignement Supérieur et de la Recherche» for the funding of XPS/LEIS/ToF-SIMS spectrometers within the Pôle Régional d'Analyses de Surface and X-Ray diffractometers. The authors would like to thank Olivier Gardoll, Laurence Burylo and Martine Trentesaux for conducting H_2 -TPR, XRD and XPS respectively.

References

- [1] Ad hoc working group on defining critical raw materials, Report on critical raw material for the E.U. (2014).
- [2] S. Royer, D. Duprez, F. Can, X. Courtois, C. Batiot-Dupeyrat, S. Laassiri, H. Alamdar, *Chem. Rev.* 114 (2014) 10292–10368.
- [3] K. Ji, H. Dai, J. Deng, L. Song, B. Gao, Y. Wang, X. Li, *Appl. Catal. B* 129 (2013) 539–548.
- [4] M. Sadakane, T. Horiuchi, N. Kato, K. Sasaki, W. Ueda, *J. Solid State Chem.* 183 (2010) 1365–1371.
- [5] H. Tanaka, M. Misra, *Curr. Opin. Solid State Mater. Sci.* 5 (2001) 381–387.
- [6] C.H. Kim, G. Qi, K. Dahlberg, W. Li, *Science* 327 (2010) 1624–1627.
- [7] C. Constantiou, W. Li, G. Qi, W.S. Epling, *Appl. Catal. B* 134–135 (2013) 66–74.
- [8] H. Tanaka, M. Uenishi, I. Tan, I. Kimura, J. Mizuki, Y. Nishihata, *SAE Paper*, 2001, 2001-01-1301.
- [9] A. Schoen, C. Dujardin, J.-P. Dacquin, P. Granger, *Catal. Today* 258 (2015) 543–548.
- [10] Y. Nishihata, J. Mizuki, H. Tanaka, M. Uenishi, M. Kimura, *J. Phys. Chem. Solids* 66 (2005) 274–282.
- [11] Y. Nishihata, J. Mizuki, T. Akao, H. Tanaka, M. Uenishi, M. Kimura, T. Okamoto, N. Hamada, *Nature* 418 (2002) 164–166.
- [12] D. Mukai, Y. Izutsu, Y. Sekine, *Appl. Catal. A* 458 (2013) 71–81.
- [13] M. Taniguchi, H. Tanaka, M. Uenishi, I. Tan, Y. Nishihata, J. Mizuki, H. Suzuki, K. Narita, A. Hirai, M. Kimura, *Top. Catal.* 42 (2007) 367–371.
- [14] H. Tanaka, I. Tan, M. Uenishi, N. Kajita, M. Taniguchi, K. Kaneko, S. Mitachi, M. Kimura, K. Narita, N. Sato, Patent EP1728766A1, 2006.
- [15] R. Hatfield, Patent WO2014/197773A1, 2014.
- [16] K. Zhou, H. Chen, Q. Tian, Z. Hao, D. Shen, X. Xu, *J. Mol. Catal. A* 189 (2002) 225–232.
- [17] S.A. Malamis, R.J. Harrington, M.B. Katz, D.S. Korschner, S. Zhang, Y. Cheng, L. Xu, H.-W. Jen, R.W. McCabe, G.W. Graham, X. Pan, *Catal. Today* 258 (2015) 535–542.
- [18] G.C. Mondragón Rodríguez, K. Kelm, S. Heikens, W. Grünert, B. Saruhan, *Catal. Today* 184 (2012) 184–192.
- [19] Y. Wu, C. Dujardin, C. Lancelot, J.-P. Dacquin, V. Parvulescu, M. Cabié, C.R. Henry, T. Neisius, P. Granger, *J. Catal.* 328 (2015) 236–247.
- [20] J.-P. Dacquin, C. Lancelot, C. Dujardin, C. Cordier-Robert, P. Granger, *J. Phys. Chem. C* 115 (2011) 1911–1921.

[21] A. Schön, J.-P. Dacquin, C. Dujardin, P. Granger, *Top. Catal.* 60 (3) (2017) 300–306.

[22] Y. Wu, X. Ni, A. Beaureain, C. Dujardin, P. Granger, *Appl. Catal. B* 125 (2012) 149–157.

[23] H. Taguchi, S. Matsu-ura, M. Nagao, T. Choso, K. Tabata, *J. Solid State Chem.* 129 (1997) 60–65.

[24] I. Twagirashema, M. Engelmann-Pirez, M. Frere, L. Burylo, L. Gengembre, C. Dujardin, P. Granger, *Catal. Today* 119 (2007) 100–105.

[25] (a) J. Rodriguez-Carvajal, *Physica B* 192 (1993) 55; (b) J. Rodriguez-Carvajal, Commission on Powder Diffraction (IUCr), *Newsletter* 26 (2001) 12–19.

[26] D.A. Shirley, *Phys. Rev. B* 5 (1972) 4709–4714.

[27] P. Granger, V.I. Parvulescu, S. Kaliaguine, W. Prellier, *Perovskites and Related Mixed Oxides: Concepts and Applications*, Wiley-VCH edition, 2016.

[28] R. Zhang, A. Villanueva, H. Alamdari, S. Kaliaguine, *J. Mol. Catal. A* 258 (2006) 22–34.

[29] F. Amano, T. Tanaka, T. Funabiki, *J. Mol. Catal. A* 221 (2004) 89–95.

[30] M.C. Biesinger, L.W.M. Lau, A.R. Gerson, R. St. C. Smart, *Appl. Surf. Sci.* 257 (2010) 887–898.

[31] S. Ponce, M.A. Peña, J.L.G. Fierro, *Appl. Catal. B* 24 (2000) 193–205.

[32] R.J.H. Voorhoeve, J.P. Remelka, L.E. Trimble, *The Catalytic Chemistry of Nitrogen Oxides*, Plenum Press, New York, 1975, pp. p215.

[33] Z. Gao, H. Wang, H. Ma, Z. Li, *J. Alloy Comp.* 646 (2015) 73–79.

[34] P. Ciambelli, S. Cimino, L. Lisi, M. Faticanti, G. Minelli, I. Pettiti, P. Porta, *Appl. Catal. B* 33 (2001) 193–203.

[35] R.D. Zhang, H. Alamdari, S. Kaliaguine, *J. Catal.* 242 (2006) 241–253.

[36] A. Schoen, Ph'Dissertation, Université Lille1, Sciences et Technologies., 2015.

[37] E. Garcia-López, G. Marci, F. Puelo, V. La Parola, L.F. Liotta, *Appl. Catal. B* 178 (2015) 218–225.

[38] T. Nakamura, M. Misono, Y. Yoneda, *Bull. Chem. Soc. Jpn.* 55 (1982) 394–399.

[39] H. Falcón, M.J. Martínez-Lope, J.A. Alonso, J.L.G. Fierro, *Appl. Catal. D* 26 (2000) 131–142.

[40] H. Arai, T. Yamada, K. Eguchi, T. Seiyama, *Appl. Catal.* 26 (1986) 265–276.

[41] B. Saruhan, G.C. Mondragón Rodríguez, A.A. Haidry, A. Yüce, S. Heikens, W. Grüner, *Adv. Eng. Mater.* 18 (2016) 728–738.

[42] I. Twagirashema, M. Frere, L. Gengembre, C. Dujardin, P. Granger, *Top. Catal.* 42–43 (2007) 171–176.